Journal of The Electrochemical Society, **159** (2) K46-K49 (2012)
0013-4651/2012/159(2)/K46/4/$28.00 © The Electrochemical Society

Enhancing Charge Collection in Dye-Sensitized Solar Cells by Trimming Sidewall of the TiO_2 Nanotubes

Yu Yen Kuo,[a] Jui Guo Lin,[a] and Chao Hsin Chien[a,b,z]

[a]*Department of Electronics Engineering, National Chiao Tung University, Hsinchu 30010, Taiwan*
[b]*National Nano Device Laboratories, 30050 Hsinchu, Taiwan*

The morphological properties of TiO_2 nanotube heavily influence the performance of dye-sensitized solar cell using TiO_2 nanotube-array as the photoanode. We report an efficient trimming method of fabricating 18.8 μm TiO_2 nanotube-arrays with sidewall thicknesses ranged from 23 nm to 12 nm. With the photoanode of thin-wall nanotube-array, the photocurrent density of the dye-sensitized solar cell increased from 13.0 mA/cm^2 to 16.2 mA/cm^2 when the thickness of the sidewall was thinned down from 23 nm to 14 nm. Electrical impedance spectroscopy showed a significant difference of internal electrical characteristics between the solar cells with the as-prepared and with thin-wall nanotube-arrays. The thinning of the sidewall of the nanotubes had little influence on the diffusion of the electrons; the improvements in photocurrent density are the result of the more efficient infiltration of electrolyte into wider voids between neighboring thin-wall nanotubes.
 [DOI: 10.1149/2.099202jes]

Manuscript submitted October 5, 2011; revised manuscript received November 15, 2011. Published December 20, 2011.

Recently, dye-sensitized solar cells (DSSC) have attracted a significant amount of attention as an efficient and low cost photovoltaic system.[1,2] Many dyes have been reported to achieve greater than 10% energy conversion efficiency when an optimized TiO_2 nanoparticle structure is used as a photoanode, providing highly efficient electron collection when the active layer is less than 10 μm.[3–5] The finite thickness of the TiO_2 photoanode due to the limited electron diffusion length in TiO_2 nanoparticles heavily restricts the performance of the DSSC. Accordingly, one dimensionally oriented TiO_2 nanostructures, such as nanofibers, nanorods, nanowires or nanotubes have been proposed as an alternative to replace the disordered TiO_2 nanoparticles, taking advantage of an enhanced charge transport ability that can increase the effective diffusion length of the photoanode of the DSSC.[6–8] Among the various nanostructures, vertically aligned and highly compact TiO_2 nanotube-arrays can be rapidly and uniformly fabricated in a large area by anodization of a Ti substrate.[9–11] Applying the anodized nanotube-array as the photoanode of DSSC leads to 7–8% energy conversion efficiency in a front-side illuminated structure, 6–7% in a back side illumination mode and 8–9% in a nanoparticle-nanotube composite structure.[12–17]

So far, various anodization conditions for preparing the nanotube-array, different post treatments to modify the surface properties of the nanotubes and their influences on the performance of the dye-sensitized nanotube solar cell (ntDSSC) have been widely studied and optimized for enhanced photovoltaic performance.[12,16–21] However, the effect of the sidewall thickness of the anodized TiO_2 nanotubes on the performance of the ntDSSC was rarely researched in the past. Since the formation of the sidewall of the anodized nanotube is the equilibrated state between the field-assisted oxide growth and the oxide dissolution, the sidewall thickness is increased in the anodization when higher potential is applied for increased growth rate of the nanotubes, so controlling the sidewall thickness of anodized nanotubes is uneasy. Especially, a thin sidewall thickness of anodized nanotubes usually cannot be achieved for a stable structure of long nanotubes when the as-anodized nanotube is usually amorphous.[22] In general, fabricating a nanotube-array over 20 μm in length with a sidewall thickness less than 20 nm is very challenging.

Herein, we report a post dissolving method to trim the sidewall thickness of the anodized nanotube-array, and the fabrication of anodized nanotube-array with a sidewall thickness less than 15 nm becomes much easy. The post dissolving process only trimmed the sidewall of the nanotubes but did not shorten the nanotubes. Utilizing the thin-wall nanotube-array as the photoanode to fabricate the ntDSSCs in the front-side illuminated architecture lead to a clear improvement in the open-circuit voltage and the short-circuit photocurrent density. The energy conversion was made with 7.9% efficiency on the ntDSSC using nanotubes with a sidewall thickness of 14nm. Results of the impedance spectroscopy analyzes showed that the thinning of the sidewall of the nanotubes has a significant impact on the internal characteristics of the ntDSSC and results in the further enhanced photovoltaic performance.

Experimental

The preparation of the TiO_2 nanotube with a trimmed sidewall followed the following procedure: First, the Ti foil (0.25 mm, Aldrich) was ultrasonically cleaned by isopropanol and de-ionized water. The anodization of the Ti foil was carried out in a solution containing 0.3 wt% NH_4F and 2 vol% water in ethylene glycol at 50 V with platinum serving as the counter electrode. The anodized TiO_2 nanotube-array was then calcined at 370°C for 3 h. After the calcination, CHF_3/CF_4 plasma was applied to the calcined sample to clean the disordered ends of the nanotube-array. Next, the nanotube-array was immersed into diluted HCl solution at room temperature for 10 min to fabricate a nanotube with a thinner sidewall thickness, and the trimmed nanotube-array was crystallized at 450°C for 3 h. Finally, secondary anodization was applied to the crystallized sample for 30 min, and the crystallized nanotube-array was detached from the Ti substrate after immersing the sample into 1.0 M HCl solution. The morphological properties of the nanotube was identified by field emission scanning electron microscopy (FESEM, Hitachi S-4700I), and the crystalline properties of the nanotube with different sidewall thicknesses were characterized by X-ray diffraction (XRD).

In order to fabricate the ntDSSC in the frontside illumination mode, the freestanding nanotube-array was bonded to a glass substrate first. A solution of 0.2 M titanium isopropoxide in acetic acid was mixed with poly ethylene glycol (MW2000) in a 10:3 mass ratio and then dripped onto the conductive glass substrate (FTO, 15 Ω/□) as the glue. Then, the freestanding nanotube membrane was put on the FTO and annealed at 450°C for 1h to make a tight bond. Next, the fabricated photoanode was immersed into 3×10^{-4} M dye (N719, Solaronix) solution for 24 h. To measure the amount of the dye molecules adsorbed by the nanotubes, the sample was immersed into 5×10^{-3} M KOH solution for desorption, and the dye concentration was measured by the UV-Vis spectroscopy.

The dye-adsorbed photoanode was dried and then encapsulated by injecting an electrolyte containing 0.05 M I_2, 0.1 M LiI, 0.5 M 4-tert-butylpyridine and 0.6 M 1-propyl-3-methylimidazolium in 3-methoxypropionitrile into the space between the FTO and the counter electrode, which is Pt coated FTO; a 60 μm spacer (SX-1170-60) was used to separate the two electrodes.

[z] E-mail: chchien@faculty.nctu.edu.tw

The photovoltaic characteristic of the ntDSSC under 100 mW/cm^2 illumination was measured by a sourcemeter (Keithley 2400); the illumination was provided by a solar simulator (Oriel) with an air mass filter. The impedance spectroscopy was measured by a potentiostat (model 273a, EG&G) equipped with a frequency response analyzer (model 1025, EG&G). For photocurrent transient measurement, the ntDSSC was illuminated by a pulsed red-light LED under steady illumination provided by a white-light LED array; the photocurrent was amplified and recorded by a digital oscilloscope.

Results and Discussion

Fig. 1 shows the FESEM images of the as-prepared nanotube-array and the nanotube-arrays after sidewall trimming in diluted HCl of different concentrations. The sidewall thickness of the nanotube varies from 23 nm to 12 nm on average after being treated by 1.0 M hydrochloric acid for 10min whereas the length remained at 18.8 μm. Noticeably, the first calcination at 370°C for the as-prepared nanotube was essential for thinning so the sidewall of the calcined TiO_2 nanotubes could be more uniformly dissolved in the acid. For first calcination at temperature lower than 370°C, the dissolution rate of the sidewall of the nanotubes in HCl became too fast; for 350°C calcined nanotubes, an apparently shortened tube length from 18.8 μm to 12.0 μm after the treatment of 1 M HCl for 10 min was observed.

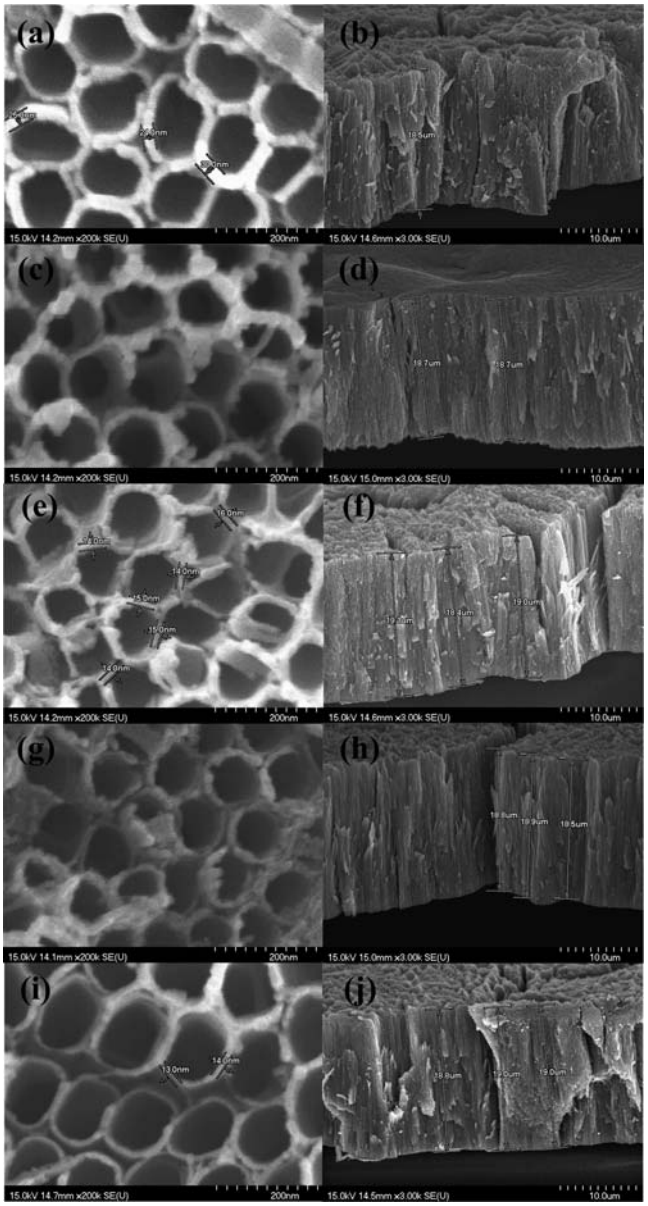

Figure 1. (a, b) The top-view and cross-section FESEM images of the as-anodized TiO_2 nanotube-array and the images of the nanotube-array trimmed by HCl of different concentrations: (c, d) 0.25 M, (e, f) 0.5 M, (g, h) 0.75 M, and (i, j) 1.0 M).

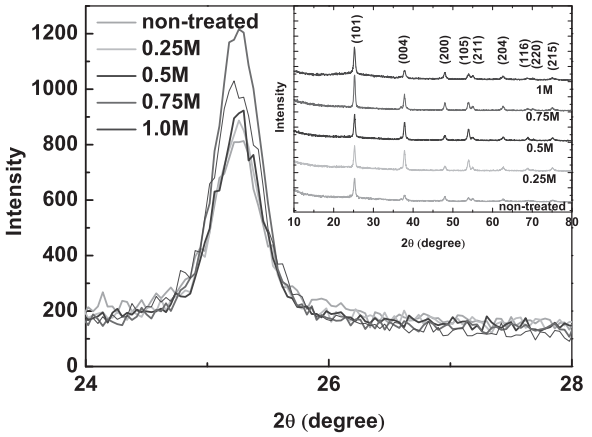

Figure 2. The X-ray diffraction results of the thin-wall TiO_2 nanotube-array trimmed by diluted HCl of various concentrations. The peaks labeled in the inserted figure represent the peaks of anatase phase.

Fig. 2 depicts the XRD spectra of the thin-wall nanotubes after the crystallization. The crystalline phase remained as the pure anatase phase for all samples, and the intensity of the (101) plane gradually increased with increasing HCl concentration and the full width at half maximum was not changed except for the one trimmed by 1.0 M HCl. The sidewall thickness of the 1.0 M HCl trimmed nanotube was about 12 nm. With such a thin sidewall, we found that the structure of the tube ends was more unstable and would collapse easily to produce additional debris on the top of nanotubes. This could be the reason for the decreased diffraction intensity. For nanotubes trimmed by 0.25 M, 0.5 M and 0.75 M HCl, the improved crystallinity of the thin-wall nanotube could result from the increasing surface-to-bulk ratio and the surface tension, which have been known to be determinative factors in the crystallization of TiO_2 nanoparticles.[23] Additionally, a significant enhancement on the intensity of (004) plane (the second peak at 37.9° in the inserted figure in Fig. 2) was found for the thin-wall nanotubes as well, which is similar to the reported result of the TiO_2 nanosheet.[24]

The photocurrent-voltage curves of the ntDSSCs with different tube sidewall thicknesses are shown in Fig. 3, and the photovoltaic

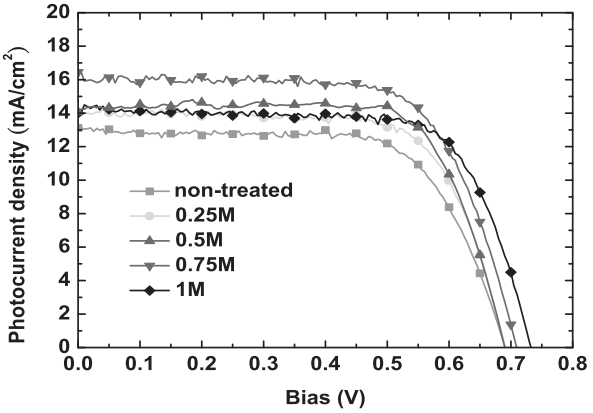

Figure 3. The photocurrent – voltage characteristics under 100 mW/cm^2 illumination of thin-wall ntDSSCs trimmed by HCl of different concentrations.

Table I. The photovoltaic parameters and the dye load of the thin-wall ntDSSCs trimmed by 0 M, 0.25 M, 0.5 M, 0.75 M and 1.0 M HCl.

Trimming condition	Dye load (10^{-7} mol/cm^2)	J_{sc} (mA/cm^2)	V_{oc} (V)	FF	η (%)
None	2.65	13.0	0.69	0.68	6.1
0.25 M	2.36	14.2	0.69	0.69	6.8
0.5 M	2.41	14.6	0.69	0.73	7.3
0.75 M	2.69	16.2	0.71	0.69	7.9
1.0 M	2.73	14.5	0.73	0.71	7.5

parameters are summarized in Table I. When the sidewall thickness of the nanotube was reduced from 23 nm to 12 nm, the open-circuit voltage increased from 0.69 V to 0.73 V. The enhancement of the open-circuit voltage is the result of the increased concentration of excess electrons on the conduction band of the thin-wall nanotubes. Table I includes the measured dye load. There was no significant variation on the dye load for the nanotube-arrays with different sidewall thicknesses. This suggested a similar amount of the excess electrons injected from the excited dye molecules. As a result, the concentration of the excess electrons increased as the total volume was reduced, and the raised quasi-Fermi level of the TiO_2 lead to a higher open-circuit voltage.

On the other hand, we noticed that there was significant enhancement of the photocurrent density of the thin-walled ntDSSC, shown in Fig. 3. In an attempt to understand the reason for the improvement, electrical impedance spectroscopy of the ntDSSCs was investigated; Fig. 4a shows the Nyquist plot of the ntDSSCs and each solid line curve is the fitting result based on the transmission line model shown in Fig. 4b: The parameters r_w, r_k and c_k are respectively the transport resistance per unit length, the recombination resistance per unit length and the chemical capacitance per unit length. Table II summarizes the electrical parameters of the fitting curves whereas $R_w = r_w L$, $R_k = r_k/L$, $C_\mu = c_\mu L$, L is the tube length, which are all 18.8 μm for these cells, and $\omega_k = R_k C_\mu$ is the effective charge transfer rate across the nanotube/electrolyte interface. Also included in Table II, the R_D and ω_i are parameters of the finite Warburg impedance element shown in Fig. 4b, as

$$W_D = R_D \frac{1}{\sqrt{i\omega/\omega_i}} \tanh\left(\sqrt{i\omega/\omega_i}\right) \quad [1]$$

Important characteristics of the thin-wall ntDSSCs could be clearly identified from these parameters. First, the transport resistance R_w was sequentially increased from 28.9 Ω to 47.0 Ω when the sidewall was trimmed. The magnitude of R_w is inversely proportional to the effective area according to the equation

$$R_w = \frac{k_B T}{q^2 A n_s} \frac{L}{D} \quad [2]$$

where k_B, T, q, L, D, A and n_s are the Boltzmann constant, temperature, elemental charge, the length of the TiO_2, the diffusion coefficient of electrons, effective area and the concentration of conduction electrons respectively. The effective area in this case refers to the total

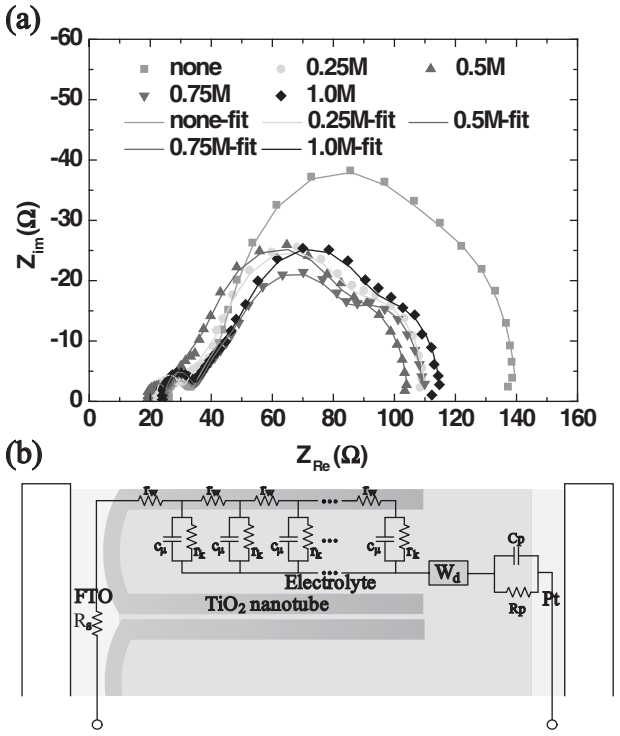

Figure 4. (a)The Nyquist plots of thin-wall ntDSSCs trimmed by HCl of different concentrations; the cells were measured at open-circuit voltage under 100 mW/cm^2 illumination. (b) The transmission line model applied for the fitting of the impedance results of the ntDSSCs.

cross sectional area of the nanotube walls rather than the conventional notation of the electrode area in nanoparticle DSSCs.[25,26] It is noteworthy that this modification is significant in evaluating the value of R_w in ntDSSCs, especially for the thin-wall ntDSSCs. Obviously, the cross sectional area of the nanotube walls in the array is the realistic transport area of electrons. Besides the decrease in effective area as the wall thickness decreased, the concentration of the conduction electrons, n_s, also increased at the same time due to the nanotube volume reduction. As a result, the value of R_w increased at a slower rate than the effective area decreased.

In contrast to the increased R_w, the diffusion resistance R_D of the iodine ions decreased when the sidewall was thinned. This is straightforward because the inner pore of the nanotubes and the voids among the nanotubes both widened after the trimming process, and the transport resistance of the ions within the nanotubes was hence lower. Moreover, because of the widening of the voids, the electrolyte could more easily infiltrate into the deep voids. This could result in the apparent decreased recombination resistance R_k and the simultaneously increased chemical capacitance C_μ since the contact area between the nanotube-array and the electrolyte became larger. The more infiltrated

Table II. The fitted parameters for impedance spectroscopy of thin-wall ntDSSCs. The active area of the cells for the impedance measurement was 2.5 mm × 2.5 mm.

Trimming condition	R_s (Ω)	R_p (Ω)	C_p (10^{-6} F)	R_w (Ω)	R_k (Ω)	C_μ (10^{-3} F)	ω_k (s^{-1})	R_D (Ω)	ω_i (s^{-1})
None	26.1	5.82	2.97	28.9	61.7	1.5	11	36.8	0.71
0.25 M	21.6	7.46	3.56	35.9	40.3	1.6	15	29.5	0.57
0.5 M	19.1	4.89	3.64	40.1	41.5	1.6	15	26.2	0.63
0.75 M	24.6	8.42	3.31	42.7	32.6	1.9	16	30.6	0.51
1.0 M	23.9	8.76	3.08	47.0	41.3	1.4	17	26.4	0.69

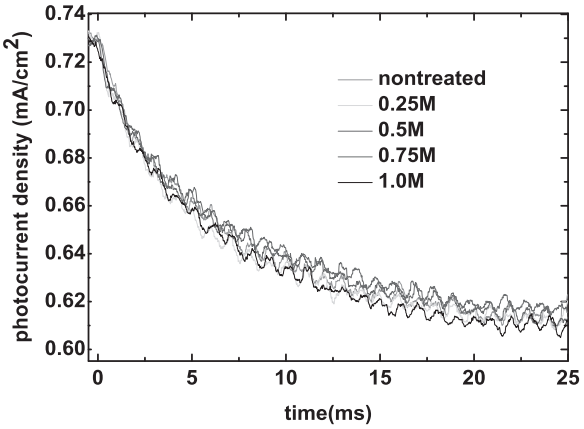

Figure 5. The short-circuit photocurrent transient results of the thin-wall ntDSSCs trimmed by HCl of different concentrations.

electrolyte and the more easily transported ions were suggested to be the main reason for the improvement on the photocurrent density.

Although the open-circuit voltage was raised as the sidewall thickness of the nanotubes was trimmed to 12 nm by 1.0 M HCl, the photocurrent density was lower in comparison to that of the sample with 0.75 M HCl treated nanotubes. One possible reason for the lowering of photocurrent density might be due to the ease of debris formation of the nanotubes as mentioned before. The debris possibly interrupted the infiltration of the electrolyte into the voids and led to the increased R_k and decreased C_μ even though the nanotube was not shortened at all.

Another interesting characteristic is the diffusion coefficient or the mobility of electrons in the thin-wall nanotubes; although apparent increase on transport resistance was observed according to impedance spectroscopy, it was still not clear whether it is mainly caused by the decreased transport area or the variation on diffusivity. In order to clarify the cause, the transient behaviors of the photocurrent of the thin-wall ntDSSCs were measured, with the results shown in Fig. 5. The diffusion time of the excess charge in the nanotubes with different sidewall thicknesses showed no obvious difference at the same photocurrent level. This result indicated that the collection of excess electrons injected from the excited dyes should not be influenced by the sidewall thickness of nanotubes since the collection of the electrons is primarily dominated by the diffusion of excess electrons when the sidewall thickness was thinner that of the space charge layer, which is approximately 30 nm.[27] Therefore, an improved photocurrent was obtained for the ntDSSCs with thin-wall nanotubes due to the further infiltration of electrolyte even though the electron transport resistance increased.

Conclusions

An anodized nanotube-array with a uniformly thinned sidewall was fabricated by etching the nanotubes after a low temperature calcination process. There was no observable shortening of the nanotubes during the application of a moderate acidic concentration and treating period. We applied the thin-wall nanotube-arrays as the photoanode to fabricate the front-side illuminated dye-sensitized solar cells. The open-circuit voltage was observed to raise due to the increased concentration of excess electrons in the thin-wall nanotubes, and impedance analyzes led to the conclusion that the significant improvement of the photocurrent resulted from the improved infiltration of electrolyte into the voids between the nanotubes. No significant influence was observed on the diffusion characteristics of the electrons inside the nanotubes that had a sidewall thickness of 23 nm to 12 nm. Based on these results, we believe the application of the thin-wall nantube-array should be essential on enhancing the overall performance of the solar cell especially when a highly viscous or quasi-solid hole transferring medium is introduced for a long term stable solar cell.

Acknowledgments

We are grateful to the National Device Laboratory for supporting XRD measurements, and acknowledge Nano Facility Center at NCTU for the use of the SEM and the sputtering system. Especially, we thank M.Y. Lee for support and assistance on electrochemical systems.

References

1. B. O'Regan and M. Grätzel *Nature*, **353**, 737 (1991).
2. A. Hagfeldt, G. Boschloo, L. Sun, L. Kloo, and H. Pettersson, *Chem. Rev.*, **110**, 6595 (2010).
3. M. K. Nazeeruddin, F. De Angelis, S. Fantacci, A. Selloni, G. Viscardi, P. Liska, S. Ito, B. Takeru, and M. Grätzel, *J. Am. Chem. Soc.* **127**, 16835 (2005).
4. S. Q. Fan, C. Kim, B. Fang, K. X. Liao, G. J. Yang, C. J. Li, J. J. Kim, and J. Ko, *J. Phys. Chem. C*, **115**, 7747 (2011).
5. T. Bessho, S. M. Zakeeruddin, C. Y. Yeh, E. W. G. Diau, and M. Grätzel, *Angew. Chem. Int. Ed.*, **49**, 6646 (2010).
6. M. Law, L. E. Greene, J. C. Johnson, R. Saykally, and P. Yang, *Nat. Mater.*, **4**, 455 (2009).
7. J. Jiu, S. Isoda, F. Wang, and M. Adachi, *J. Phys. Chem. B*, **110**, 2087 (2006).
8. A. Mathew, G. M. Rao, and N. Munichandraiah, *Mater. Chem. Phys.*, **127**, 95 (2011).
9. G. K. Mor, K. Shankar, M. Paulose, O. K. Varghese, and C. A. Grimes, *Nano Lett.*, **6**, 215 (2006).
10. K. Zhu, N. R. Neale, A. Miedaner, and A. J. Frank, *Nano Lett.*, **7**, 69 (2007).
11. J. Wang and Z. Q. Lin, *J. Phys. Chem. C*, **113**, 4026 (2009).
12. C. C. Chen, H. W. Chung, C. H. Chen, H. P. Lu, C. M. Lan, S. F. Chen, L. Luo, C. S, Hung, and W. G. Diau, *J. Phys. Chem. C*, **112**, 19151 (2008).
13. O. K. Varghese, M. Paulose, and C. A. Grimes, *Nat. Nanotechnol.*, **4**, 592 (2009).
14. C. J. Lin, W. Y. Yu, and S. H. Chien, *J. Mater. Chem.*, **20**, 1073 (2010).
15. B. X. Lei, J. Y. Liao, R. Zhang, J. Wang, C. Y. Su, and D. B. Kuang, *J. Phys. Chem. C*, **114**, 15228 (2010).
16. Q. Zheng, H. Kang, J. Yun, J. Lee, J. H. Park, and S. Baik, *ACS Nano*, **5**, 5088 (2011).
17. J. Wang and Z. Q. Lin, *Chem. Mat.*, **22**, 579 (2010).
18. S. H. Kang, J. Y. Kim, Y. Kim, H. S. Kim, and Y. E. Sung, *J. Phys. Chem. C*, **111**, 9614 (2007).
19. X. Pan, C. Chen, K. Zhu, and Z. Fan, *Nanotechnology*, **22**, 235402 (2011).
20. M. Ye, X. Xin, C. Lin, and Z. Lin, *Nano Letters*, **11**, 3214 (2011).
21. J. R. Jennings, A. Ghicov, L. M. Peter, P. Schmuki, and A. B. Walker, *J. Am. Chem. Soc.*, **130**, 13364 (2008).
22. G. K. Mor, O. K. Varghese, M. Paulose, K. Shankar, and C. A. Grimes, *Sol. Energy Mater. Sol. Cells*, **90**, 2011 (2006).
23. A. S. Barnard, and L. A. Curtiss, *Nano Lett.*, **5**, 1261 (2005).
24. X. Wei, J. Liu, Y. Z. Chua, J. Song, and X. W. Liu, *Energy Environ. Sci.*, **4**, 2054 (2011).
25. M. Adachi, M. Sakamoto, J. Jiu, Y. Ogata, and S. Isoda, *J. Phys. Chem. B*, **110**, 13872 (2006).
26. J. Bisquert, G. Belmonte, F. Santiago, N. S. Ferriols, P. Bogdanoff, and E. C. Pereira, *J. Phys. Chem. B*, **104**, 2287 (2000).
27. L. Sun, S. Zhang, X. Sun, and X. J. He, *Nanosci. Nanotechnol.*, **10**, 4551 (2010).